Original Reviews

Anonymous Referee #1:

This paper presents a potentially valuable new data set that uses microwave SST data to map the position of the Polar Front of the Antarctic Circumpolar Current. The position of the front is a valuable indicator of ACC meandering, and there will undoubtedly be quite a bit of interest in working with this data set.

Unfortunately, the presentation in the paper is lean on the details that readers will need in order to understand and use the data set.

To my mind, the core of a data paper is the methods section, which explains how the data set was generated. In this case, the methods section doesn't provide enough information. - In section 2.2.1, the SST gradient is defined for Delta T, but the units don't make sense. Perhaps it's supposed to be a gradient of T (i.e., nabla T)? This should be explained carefully. **1**
- In section 2.2.2, continuity tests are discussed. The basic terms seem to be inadequately defined. For example d is used to represent differences, l latitude, and t temperature, but the scale over which d_l is calculated is not clear. d_tc is used but not clearly defined. The **2**
main definition of the algorithm, at the top of p. 4, considers multiple cases, but it's not clear what the role of each of the cases is. Why is the case sigma_l = d_l considered, since **3**
it's unlikely that any real world variables would be equal. In the event that they are equal, couldn't this be the limiting case for sigma_l < d_l, for example?

What sets sigma_l > 0.75 as a criterion for possibly adjusting the PF position? Why not a **4**
different limit? What are the units of 0.75.

Why is the condition d_l(west) < sigma_l < d_l(east) considered, but not the opposite (d_l(east) < sigma_l < d_l(west))? Later the text says that some regions are processed from east to west rather than west to east, so perhaps that is part of the explanation. But **5**
that still leaves me wondering why there is an asymmetry in the mapping? Wouldn't the algorithm seem more robust if it applied criteria in both directions?

- Why are the particular regions in section 2.2.4 identified to be analyzed from east to west, **6**
rather than west to east? What makes these regions different?

- The presentation of the algorithm in its present form makes the algorithm seem like it has been hacked together by adding extra cases until it works, and this does not inspire confidence that the algorithm will work reliably in all cases. Can it be simplified? The big **7**
concern is cases when d exceeds sigma, so why worry about the d < sigma cases at all? Why do Delta_t > 1 and d_t > sigma_t both need to be set as criteria? Please explain for your readers.

- The validation in section 3 leaves open a number of questions as well. What do XBTs offer that satellite SST does not? Should the XBTs agree with SST, or are they measuring **8**

different quantities?

- Root-mean-squared differences between the XBT Polar Front and the SST Polar Front are computed. The manuscript reports "high RMSE values" in some regions. What makes the RMSE high – what would be a low RMSE value? The manuscript also says that the PF positions "give a reasonable PF location." What is the metric for deciding that the PF positions are reasonable? How much uncertainty should someone expect? I think Dong et al show the standard deviation of PF latitude, and that might be a helpful metric here for evaluating the range of variability. **9**

- In section 4, the discussion of Figure 5 reports that the parameters of the PF are closely linked to the depth of the topography. What is the evidence for this? Some studies would argue that the gradient of topography should matter or that flow should follow contours of f/H. Can the manuscript be more specific about the role of topography? It's hard to draw firm conclusions by comparing Figure 5d (depth) with the other panels of Figure 5. **10**

In general, why are the algorithms structured the way they are? Why use these particular temperature and latitude criteria? **11**

- It's a bit unusual to define sigma to be twice the standard deviation, and I think readers are likely be confused by this. If twice the standard deviation is used, I would refer to that as 2 sigma. **12**

Finally, the writing is a bit rough in places and should be edited carefully. **13**

The data set itself is readable, and can be downloaded and plotted without difficulty. **14**

G. M. R. Manzella, Referee #2:

The paper is of interest for an area of oceanographic importance such as the ACC. There are some points to be clarified in the paper. The PF identification procedures must eliminate the eddies. **15** The paper is stating that the PF procedure is not applied to areas where the SST gradient is having certain characteristics (para 2.2.1, 23-25). This choice is not explained in the paper. **16** Furthermore, the authors should discuss (1) if and how temporal and spatial variability of eddies can influence the results (2) if a filter should be applied to data or (3) the proposed methodology is avoiding biases due to eddies. **17**

Response to Reviewers and Proposed Revisions

We thank the reviewers for the constructive comments which have substantially improved our original manuscript. In response to these comments, we propose the following changes for the revised manuscript.

Reviewer #1

1 The units of the SST gradient (ΔT) are °C/km (simplification outlined below). To ensure the reader's understanding, we have added explicit units in the text (see below).

$$|\Delta T| = \sqrt{(^\circ C/km)^2 + (^\circ C/km)^2},$$

$$|\Delta T| = \sqrt{(^\circ C/km)^2},$$

$$|\Delta T| = (^\circ C/km).$$

Revised manuscript, section 2.2.1:
"South of 40° S, we compute the absolute SST gradient ***(° C km^{-1})*** *at each grid point,*

$$|\Delta T| = \sqrt{(\delta T/\delta x)^2 + (\delta T/\delta y)^2},$$

where δT is the temperature difference ***(° C)*** *and δx and δy are the kilometer distances between any two longitude or latitude points, respectively."*

2 Indeed, d is used to represent the difference in latitude (l) or temperature (t). The scale over which these variables are calculated are degrees latitude and °C, respectively. We have now included explicit units in the text (see below). Additionally, d_{tc} is the difference in monthly climatological temperature (tc), also having units of °C. We have more clearly defined and incorporated d_{tc} (see below).

Revised manuscript, section 2.2.2:
"Starting at the Greenwich Meridian and moving east, we calculate the absolute differences (d) in latitude (l; ***° latitude****), temperature (t;* ***° C****), and monthly climatological temperature (tc;* ***° C****) between the current position and the point to the west (←) and east (→), twice the standard deviation of these differences,* ***2σ_l (° latitude)*** *and* ***2σ_t*** *and* ***2σ_{tc} (° C)*** *respectively, and an additional difference (Δ) between* ***2σ*** *and d (e.g., $\overleftarrow{\Delta}_l$ = | $\overleftarrow{d}_l$ -* ***2σ_l*** *|)."*

3 First, the reviewer has brought our attention to some missing information in the manuscript. The standard deviation is normalized by N, not N-1 as the reviewer and any reader may have assumed; we have added this key piece of information to the manuscript (see below). Indeed, given that a sample of N = 2 is used throughout, taking twice the standard deviation is the same as taking the difference of the two differences. Following this, the case $2\sigma_l = \overleftarrow{d}_l$ can indeed be satisfied and is an important metric in identifying locations where both the current position and position to the east lie at the same latitude but are separated from

the reference point to the west by more than 0.75° latitude while simultaneously violating thermal continuity (see top left panel in Figure R1).

Revised manuscript, section 2.2.2:
*"Starting at the Greenwich Meridian and moving east, we calculate the absolute differences (d) in latitude (l; °**latitude**), temperature (t; °**C**), and monthly climatological temperature (tc; °**C**) between the current position and the point to the west (←) and east (→), twice the standard deviation of these differences **(normalized by N = 2)**, **2**σ_l **(°latitude)** and **2**σ_t and **2**σ_{tc} **(°C)** respectively, and an additional difference (Δ) between **2**σ and d (e.g., $\overleftarrow{\Delta_l}$ = | $\overleftarrow{d_l}$ - **2**σ_l |)."*

4 The units of 0.75 in the $2\sigma_l > 0.75$ criterion are degrees of latitude and we have added this note explicitly in the text (see below). Using a criterion other than 0.75°latitude results in an unrealistic PF. Please see point **7** below.

Revised manuscript, section 2.2.2:
*"An adjustment in the PF position is required if **2**σ_l > 0.75 °**latitude or (**$2\sigma_l \leq$ **0.75°latitude and (**$\overleftarrow{\Delta_l}$ > **0.25°latitude or** $\overrightarrow{\Delta_l}$ > **0.25°latitude))** and any of the following are satisfied:"*

5 The conditional statements are structured to correspond with the direction one is mapping the PF. As such, the conditions outlined on page 4, line 10 are to be tested when mapping west to east, as stated in lines 2-3 on page 4. Our technique maps the front with the general eastward flow of the ACC; we have included this language in the text (see below). Indeed, some regions are processed in the reverse direction. In this case, all arrows (indicating west and east) found in the conditional statements (line 10) should be reversed.

Revised manuscript, section 2.2.2:
*"Starting at the Greenwich Meridian and moving east, **with the general flow of the ACC,** we calculate the absolute differences (d) in latitude (l; °**latitude**), temperature (t; °**C**), and monthly climatological temperature (tc; °**C**) between the current position and the point to the west (←) and east (→), twice the standard deviation of these differences **(normalized by N = 2)**, **2**σ_l **(°latitude)** and **2**σ_t and **2**σ_{tc} **(°C)** respectively, and an additional difference (Δ) between **2**σ and d (e.g., $\overleftarrow{\Delta_l}$ = | $\overleftarrow{d_l}$ - **2**σ_l |)."*

6 We explain why we map certain regions from east to west at the beginning of Section 2.2.4. We provide more specific descriptions for the reviewer below.

- ∼20-32°E: South-West Indian Ridge region is known as a "southwest eddy corridor" or "isolated eddy hotspot" (Ansorge et al., 2014), often exhibiting intense meandering (consistent with Moore et al., 1999), likely deflected southward by the ridge itself (Deacon, 1937)

- ∼50-62°E near Crozet: the sharp turn the PF path takes around Crozet is often dampened if not mapped against the flow, from east to west; here, moving south,

the PF traverses nearly 4° latitude and often requires violation of spatial continuity in order to capture the filament's southern boundary

- ∼72-80°E near Kerguelen: much like ∼50-62°E above, continuity constraints often prohibit the capture of the southernmost frontal filaments downstream of Kerguelen; by starting from 80°E and moving west, we avoid detection of the Subantarctic Front (SAF)

- ∼125-150°E along the Southeast Indian Ridge: this region is characterized by many, smaller-scale and disconnected filament structures (much like the southeast Atlantic sector; reflected in the spread of previous climatologies shown in Figure 6); in order to prevent northward or southward runoff/propagation and PF mis-identification, mapping in this region is more accurate when mapping westward from the highly constrained PF path along the Southeast Indian Ridge

- ∼170-190°E in the New Zealand sector: a persistent, disconnected, southerly filament exists around ∼180°E and in order to consistently map it despite violation of spatial/thermal continuity, mapping in the reverse is required

- ∼200-215°E along the Pacific-Antarctic Ridge: much like the reasoning behind the ∼125-150°E region above, mapping from a highly topographically-constrained region results in more consistent/accurate mapping

- ∼240-300°E in the E. Pacific: wrought with the weakest SST gradients from which to identify the location of the PF, mapping from east to west across this sector results in a more accurate representation of the southernmost frontal filaments (consistent with the mapping techniques of Dong et al., 2006b)

- ∼352-360°E along the Mid-Atlantic Ridge: as this is a region where SAF interaction occurs, the PF must be mapped starting from the more southerly position at ∼50°S at the Greenwich Meridian and moving west until it merges with the SAF

7 We thank the reviewer for their concern. Throughout algorithm development, our goal was to keep the PF mapping procedure as simple and universally-applicable as possible; to yield a robust method applicable for the entire Southern Ocean basin (1400 longitude points) and for the entire time series (612 weeks). To elucidate the four conditional statements presented on page 4, line 10 (their purpose, what they physically indicate/represent, etc.), we have created additional visual examples (Figure R1; as in Figure 1) with hopes of inspiring more confidence in these tests and to help answer many of the reviewer's comments on algorithm specifics.

The panels of Figure R1 show a typical snapshot of each of the four violations in spatial and/or thermal discontinuity. At first guess, the PF is identified as the southern bound of the 0.015°C km^{-1} SST gradient (white circles). Upon violation of any of the four conditional statements outlined on page 4, line 10, an adjustment in the first-guess PF position is

made (black plusses). Indeed, the latitude and temperature of the current position and its neighbors (one point to the west and east; three positions indicated by black open circles) are compared and if a violation has occurred, the current position is adjusted (black/gray plus) as described in Section 2.2.3. Neglecting to check for spatial and thermal discontinuity often results in a misidentified PF. For example, in the top left panel of Figure R1, we see that the first-guess PF is the SAF and therefore needs adjustment.

We now include a discussion of some advantages of our mapping procedure (see below).

Revised manuscript, section 2.2:
"We build on the technique first presented by Moore et al. (1997) of using satellite SST gradient maxima to locate the PF. In general, our PF mapping technique is based on locating the southern bound at which the SST gradient exceeds 1.5°C over a 100 km distance, as in Dong et al. (2006b). At longitudes where this criterion cannot be satisfied or when large latitudinal distances exist between adjacent longitudes, steps are taken to satisfy spatial and/or thermal continuity, oftentimes as a relaxation of the above limit (see following subsections). ***Dong et al. (2006b) use*** 2σ ***and the temporal mean PF to identify such discontinuity. Here, we identify additional physical characteristics of the PF and use this information in a comprehensive mapping scheme. Our methodology does not require knowledge of a temporal mean PF; all information needed to map the PF is found locally.*** *Our mapping scheme yields one continuous, unique PF realization for a given period of time. In regions where the PF is known to have multiple filaments (Sokolov and Rintoul, 2002), our algorithm typically selects the southernmost."*

Revised manuscript, section 2.2.2:
"Figure 1 exemplifies spatial and thermal discontinuity according to (1) and shows the subsequent adjustment made in this particular case (adjustment procedure detailed in Section 2.2.3). ***Here, black plus signs indicate the first-guess PF position (i.e., the southern bound of the 1.5 temperature gradient criterion after removing noise /patches), where the current position being tested for continuity and its immediate neighbors to the west and east are indicated by black open circles. As spatial and thermal continuity is violated in this case (see difference and standard deviation information provided in text boxes), an adjustment in the PF position is made (white plus sign).***"

8 The high-resolution spacing of XBT profiles (e.g., ∼5-10 km across Drake Passage) provides a robust, in situ way of identifying the sharp thermal gradient characterizing the PF. Due to a combination of factors, temperatures measured via XBTs will not necessarily agree with those measured from satellites. XBT data provide what is referred to as a 'bulk' SST measurement whereas microwave data provide subskin SST measurements. Dong et al. (2006a) define these terms in the following way: "...skin SST is a temperature measured by an infrared radiometer at a depth of order 0.01 mm depending on the wavelength of the measurement; subskin SST represents the temperature at the bottom of the skin SST gradient at a depth of approximately 1 mm that corresponds to the attenuation length of microwave

radiation; and foundation [or bulk] SST is the temperature free of diurnal temperature variability and is measured traditionally from temperature sensors mounted on ships and buoys at a depth of ∼1-5 m." We refer the reviewers/readers to Dong et al. (2006a), providing a detailed look at using XBT data to validate satellite-derived SSTs, including the factors that may cause differences in measured temperature.

In Section 3, as in Dong et al. (2006b), we use XBT data to validate PF position determined from microwave SSTs, and we further quantify mapping error, providing sector-specific RMSE values.

9 We use the terms "high" and "low" in reference to the magnitude of the RMSE values in a *relative* sense. However, the reviewer brings up a good point and we acknowledge that there is no absolute/clear criterion for a 'good' RMSE value; the language used in this section is too colloquial. As such, we have removed these descriptions from the manuscript and inserted more discussion on sources of error throughout the section (see below).

Revised manuscript, section 3:
"We quantify the error associated with our PF mapping scheme ***in these three regions*** *by calculating the root-mean-square error (RMSE), a measure of the* ***average magnitude of the*** *latitudinal differences between the PF inferred from XBT data (PF_X) and that from* ***weekly*** *microwave data (PF_M), as:*

$$RMSE = \sqrt{\frac{\sum_{i=1}^{n}(PF_{X,i} - PF_{M,i})^2}{n}},$$

where n corresponds to the number of transects in a given sector. Table 1 lists RMSE and sample size by sector. Transects where a meridional temperature gradient satisfying our 0.015°C km^{-1} criterion could not be identified were excluded from these calculations (8 transects in total).

Differences between in situ and satellite PF locations are likely attributed to one or more of the following: (1) interpolating XBT SSTs on to the satellite grid, (2) differences in the representative temperature measured by the two sources ('bulk' versus 'subskin'; see Dong et al., 2006a), (3) errors in the original temperature data (e.g., manufacturer, accuracy, precision, etc.), (4) the regional complexity of the front (i.e., magnitude of mesoscale variability, typical number of branches, etc.), or (5) comparing a daily in situ PF with the corresponding weekly satellite PF.

The PF within the *Australian and African sectors (****RMSE*** *1.1640 and 0.7971°* ***latitude****, respectively; 2σ = 2.33 and 2.09° latitude, respectively),* ***is known for its*** *multi-filament structure (Belkin and Gordon, 1996; Moore et al., 1999; Sokolov and Rintoul, 2002, 2009),* ***making difficult the comparison between in situ and satellite-based definitions****. For example, Figure 3a shows more than one potential frontal location along a November 2003 transect south of Australia; the in situ PF is identified as the more northerly filament while our weekly PF realization marks the more southerly filament. Figure 3c shows*

a summertime African transect where the in situ PF is identified as a more southerly filament and our weekly realization represents the northern, more spatially continuous filament. ***In*** *Drake Passage (RMSE = 0.5373°* ***latitude; 2σ = 1.47° latitude****), the PF is largely constrained by bathymetry (Moore et al., 1997) and characterized by an intense temperature gradient.* ***Figure 3b shows a summertime Drake Passage transect where the in situ and satellite PF are identified one grid box apart (0.25° latitude). Such consistent identifications are reflected in the RMSE here, where on average, our mapping technique will provide PF positions within ∼0.5° latitude of an in situ position in a given week.****"*

10 We present and discuss evidence for a link between the PF and its thermal characteristics with the depth of bottom topography in lines 19-23 and 29-33 on page 6 of the manuscript, results which are consistent with previous PF studies (Gille, 1994; Moore et al., 1999; Sokolov and Rintoul, 2002; Dong et al., 2006b; Sallée et al., 2008) and demonstrated in Figures 5 and 6 therein. Indeed, whether bottom topography is the dominant, controlling factor in dictating the *variability* in the PF is still a highly-debated topic. As the spatio-temporal variability in the PF and its characteristics is beyond the scope of this methods paper (for this, we direct the readers/reviewers to our in prep paper cited within the manuscript), we tackle the PF-topography relationship in a more generalized manner. Within the text, we further support this argument by providing statistically significant correlation coefficients (line 18, page 6; Figure 5). Yet, in order to be more specific about the role of topography, we have emphasized our focus (i.e., the mean), included additional discussion on the relationship between topography and potential vorticity constraints, and changed some of the language (see below).

Revised manuscript, section 4:
"Figure 5 suggests that the ***mean*** *position, temperature, and intensity of the PF are* ~~*closely*~~ *linked to the depth of the underlying topography (r = 0.43, r = 0.29, and r = 0.27, respectively), in agreement with previous PF studies (Gille, 1994; Moore et al., 1999; Sokolov and Rintoul, 2002; Dong et al., 2006b; Sallée et al., 2008). Indeed, the front tends to be southerly, cold, and weak over the deep ocean, and northerly, warm, and intense over shallow bathymetry. In the southwest Indian sector, the PF is in its northernmost position and characterized by warm SSTs (Figure 4; Figure 5a,b). Generally, the PF has a more southerly position in the deep, east Pacific sector, characterized by cooler SSTs and relatively weak SST gradients (Figure 4; Figure 5; Moore et al., 1999; Dong et al., 2006b).* ***Figure 5c demonstrates that the PF intensifies at major topographic features, which are associated with strong, large-scale potential vorticity gradients that act to constrain the flow (Gordon et al., 1978; Sallée et al., 2008), including the Kerguelen Plateau (∼ 80°E), across the Southeast Indian Ridge (∼ 150°E), Drake Passage (∼ 60° W), and the Pacific-Antarctic Ridge (∼ 140° W).****"*

11 Please see point **7** above.

12 We agree that σ throughout the manuscript should read 2σ and have made all the

appropriate changes in both the text and in Figure 1.

13 We appreciate the reviewer's comment but without more information, we could not specifically address any writing the reviewer deemed rough. We expect that the changes made to the manuscript as suggested by the reviewers improved overall readability.

14 We thank the reviewer for the confirmation.

Reviewer #2

15, 17 It is important to note that PF identification procedures presented herein *avoid* relatively smaller-scale eddies (isolated and detached areas of high SST gradients) but may on occasion deem the southern bound of a large, mesoscale eddy (50-100 km length scales) as part of the PF (having a cross-frontal spatial scale of similar order). The PF is often associated with/characterized by intense meanders and eddies that are created via instabilities in the mean flow, which can then break away from the main part of the front or continue to merge or interact with the front. Thus, removing these larger, mesoscale features could result in a misrepresentation of the front itself (Sarah Gille, pers. comm.). Ultimately, spatial and temporal variability of such eddies will likely influence our PF data most in regions where flow is not strongly steered by topography.

16 We have added additional explanation and references to improve the clarity of the PF identification procedure outlined in Section 2.2.1, lines 26-28, a-b. We feel that point (c) has adequate explanation/citation and thus left it unchanged.

Revised manuscript, section 2.2.1:
"We do not perform ***initial, first-guess*** *frontal identification (a) in regions where SST is warmer than 10°C,* ***as these are waters characteristic of the SAF (Dong et al., 2006b)****, (b) within small patches of high SST gradients (****closed contours*** *less than 3 degrees of latitude and longitude), so as to* ***reduce noise (as in Dong et al., 2006b)****, and (c) within 1 degree of latitude of the Antarctic continent or sea ice, in case of melt-influenced SSTs (Smith and Comiso, 2008)."*

References

Ansorge, I. J., Jackson, J. M., Reid, K., Durgadoo, J. V., Swart, S., and Eberenz, S. (2014). Evidence of a southward eddy corridor in the south-west Indian ocean. *Deep-Sea Res II.*

Belkin, I. M. and Gordon, A. L. (1996). Southern Ocean fronts from the Greenwich meridian to Tasmania. *Journal of Geophysical Research*, 101:3675–3696.

Deacon, G. E. R. (1937). The hydrology of the Southern Ocean. *Discovery Rep.*, XV:1–124.

Dong, S., Gille, S. T., Sprintall, J., and Gentemann, C. (2006a). Validation of the Advanced Microwave Scanning Radiometer for the Earth Observing System (AMSR-E) sea surface temperature in the Southern Ocean. *J. Geophys. Res.*, 111(C04002).

Dong, S., Sprintall, J., and Gille, S. T. (2006b). Location of the Antarctic Polar Front from AMSR-E Satellite Sea Surface Temperature Measurements. *J. Phys. Oceanogr.*, 36:2075–2089.

Gille, S. T. (1994). Mean sea surface height of the Antarctic Circumpolar Current from Geosat data: Method and application. *Journal of Geophysical Research*, 99:255–273.

Gordon, A. L., Molinelli, E., and Baker, T. (1978). Large-Scale Relative Dynamic Topography of the Southern Ocean. *Journal of Geophysical Research*, 83(C6).

Moore, J. K., Abbott, M. R., and Richman, J. G. (1997). Variability in the location of the antarctic polar front (90^o-20^ow) from satellite sea surface temperature data. *Journal of Geophysical Research*, 102(C13):27,825–27,833.

Moore, J. K., Abbott, M. R., and Richman, J. G. (1999). Location and dynamics of the Antarctic Polar Front from satellite sea surface temperature data. *Journal of Geophysical Research: Oceans*, 104(C2):3059–3073.

Sallée, J. B., Speer, K., and Morrow, R. (2008). Response of the Antarctic Circumpolar Current to Atmospheric Variability. *Journal of Climate*, 21(12):3020–3039.

Smith, W. O. and Comiso, J. C. (2008). Influence of sea ice on primary production in the southern ocean: A satellite perspective. *Journal of Geophysical Research: Oceans (1978–2012)*, 113(C05S93).

Sokolov, S. and Rintoul, S. R. (2002). Structure of southern ocean fronts at 140^oe. *Journal of Marine Systems*, 37:151–184.

Sokolov, S. and Rintoul, S. R. (2009). Circumpolar structure and distribution of the Antarctic Circumpolar Current fronts: 1. Mean circumpolar paths. *Journal of Geophysical Research*, 114(C11018).

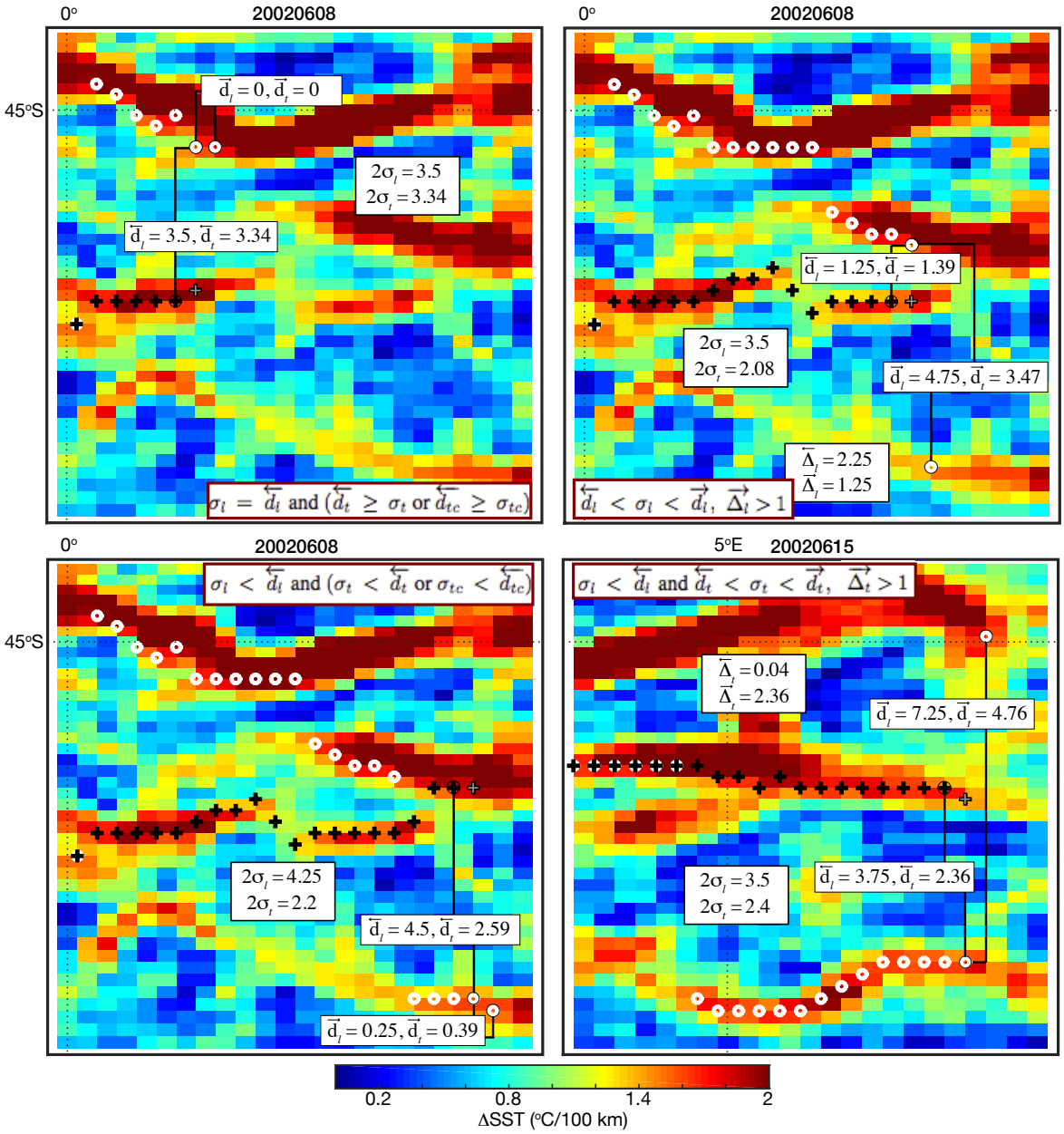

Figure R1: Examples of spatial/thermal discontinuity according to each conditional statement outlined in Section 2.2.2 and indicated in a red text box toward the center of the 4 panels. Timestamps are provided at the top of each panel. White circles indicate the first-guess PF position (solely the southern bound of the 1.5 temperature gradient after removing noise/patches), black plus signs indicate the adjusted PF positions after spatial and thermal continuity testing, the three locations outlined in a black circle are the isolated positions being tested (west, current, and east), and the gray/black plus sign represents the adjustment made in the current position.

Mapping the Antarctic Polar Front: Weekly realizations from 2002 to 2014

Natalie M. Freeman[1] and Nicole S. Lovenduski[1]

[1]Department of Atmospheric and Oceanic Sciences and Institute of Arctic and Alpine Research, University of Colorado Boulder, Boulder, CO, USA

Correspondence to: N. M. Freeman (natalie.freeman@colorado.edu)

Abstract. We map the weekly position of the Antarctic Polar Front (PF) in the Southern Ocean over a 12-year period (2002-2014) using satellite sea surface temperature (SST) estimated from cloud-penetrating microwave radiometers. Our study advances previous efforts to map the PF using hydrographic and satellite data and provides a unique realization of the PF at weekly resolution across all longitudes (http://doi.pangaea.de/10.1594/PANGAEA.855640). The mean path of the PF is asymmetric; its latitudinal position spans from 44 to 64°S along its circumpolar path. SST at the PF ranges from 0.6 to 6.9°C, reflecting the large spread in latitudinal position. The average intensity of the front is 1.7°C per 100 km, with intensity ranging from 1.4 to 2.3°C per 100 km. Front intensity is significantly correlated with the depth of bottom topography, suggesting that the front intensifies over shallow bathymetry. Realizations of the PF are consistent with the corresponding surface expressions of the PF estimated using expendable bathythermograph data in the Drake Passage and Australian and African sectors. The climatological mean position of the PF is similar, though not identical, to previously published estimates. As the PF is a key indicator of physical circulation, surface nutrient concentration, and biogeography in the Southern Ocean, future studies of physical and biogeochemical oceanography in this region will benefit from the provided data set.

1 Introduction

The large-scale circulation of the Southern Ocean (south of 35°S) is dominated by the strong, eastward flow of the Antarctic Circumpolar Current (ACC), connecting the major ocean basins and allowing for the transport of heat, nutrients, carbon, and other key climate variables globally and to the ocean interior (Rintoul et al., 2001; Sarmiento et al., 2004). The ACC is composed of many deep-reaching hydrographic fronts that divide the Southern Ocean up into physical and biogeochemical zones (see Deacon, 1982; Pollard et al., 2002). The flow of the ACC is concentrated in several jets within which the majority of the circumpolar transport is carried (Rintoul et al., 2001). The terms 'front' and 'jet' have often been used interchangeably throughout the ACC literature but are distinct features: an ACC front is a water mass boundary that is often associated with an ACC jet, a strong geostrophic current.

While as many as 10 distinct fronts can be realized in the Southern Ocean (Sokolov and Rintoul, 2007), the three majorly recognized ACC fronts are, from north to south, the Subantarctic Front (SAF), Antarctic Polar Front (PF), and southern ACC front (Orsi et al., 1995). At the PF, cold, fresh Antarctic surface waters subduct beneath warmer, saltier sub-Antarctic waters

(Deacon, 1933; Deacon, 1937). At the surface, the PF is characterized by strong gradients in temperature, nutrients, and distinct biological communities (Deacon, 1933, 1937; Mackintosh, 1946; Deacon, 1982; Trull et al., 2001). Accurately identifying the location of the PF has been an important and active area of research in recent decades as frontal position has implications for Southern Ocean eddy mean flow, air-sea fluxes, biological productivity, biogeography, and estimates of ACC transport (Hughes and Ash, 2001; Pollard et al., 2002; Sarmiento et al., 2004; Ansorge et al., 2014).

There are multiple ways to identify the PF using temperature and salinity data collected on hydrographic and bathythermographic sections. A common method uses the 2°C isotherm at ∼200 m to mark the subsurface PF, as it is a good approximation of the northern extent of cold, fresh Antarctic Surface Water that generally occupies the upper water column between the PF and the Antarctic continental shelf (Orsi et al., 1995; Belkin and Gordon, 1996). While useful in capturing the vertical structure of the PF on regional scales and over short time periods, in situ data in the Southern Ocean is spatially and temporally sparse, making difficult the study of spatiotemporal variability in the PF.

Satellites have allowed for a large-scale view of the historically under-sampled Southern Ocean. Altimeter images of sea surface height (SSH) reflect features of the upper ocean density field and gradients in SSH have been used to characterize jet intensity and front location (Gille, 1994; Sokolov and Rintoul, 2007; Sallée et al., 2008). Sokolov and Rintoul (2002) demonstrate that regions of strong SSH gradients tend to coincide with particular SSH contours and that the circumpolar path of a particular SSH contour marks the location of an ACC front. However, SSH contouring methods to identify the PF should be approached with caution: Graham et al. (2012) show that an SSH contour is not always associated with an enhanced SSH gradient, challenging the accurate detection of the time-varying front.

Given the signature strong sea surface temperature (SST) gradient at the PF, satellite images of SST can also be used to identify the PF. However, previous PF studies have used infrared retrievals of SST (Legeckis, 1977; Moore et al., 1997, 1999) which are greatly affected by water vapor and clouds, a persistent feature of the Southern Ocean. SST estimates from cloud-penetrating microwave radiometers circumvent the above PF mapping limitations, first demonstrated by Dong et al. (2006b).

Our study learns from and advances previous efforts to map the PF. Herein, we use the continuous, all-weather microwave SST record at 25 km resolution to estimate the weekly location of the PF from 2002 to 2014. As such, our method avoids water vapor and cloud contamination and provides circumpolar realizations of the PF at high spatial and temporal resolution. Our realizations of the Polar Front are made publicly available (Section 6) so as to benefit studies of Southern Ocean physical and biogeochemical oceanography (e.g., Munro et al., 2015a, b; Freeman and Lovenduski, 2015). In the following sections we detail our PF identification method (Section 2), use available expendable bathythermograph (XBT) data to test our method in select sectors of the Southern Ocean (Section 3), and discuss the mean path of the PF (Section 4). A companion paper investigates spatial and temporal variations in the PF and its linkages with key modes of climate variability (Freeman and Lovenduski, in prep.).

2 Methods

2.1 Sea surface temperature observations

In this study we utilize Remote Sensing System's daily optimally interpolated microwave SST data on a 25 km grid; daily SSTs were averaged over 7 days ending on and including the Saturday file date to create a weekly product. This all-weather SST product is derived from in situ estimates and all available microwave SST radiometers operating on a given day between 02 June 2002 and 22 February 2014: the Advanced Microwave Scanning Radiometers (AMSR-E and AMSR-2) and WindSat Polarimetric Radiometer (see Reynolds and Smith, 1994). Data processing involves many quality control measures, including the removal of rain- or sea ice- contaminated SSTs and consideration of diurnal warming and sensor error. It is important to note that there are a few instances in the data record when no radiometer was operational and the SST retrieval from the previous day is used persistently (outages range $\sim$1-7 days). For further details on data processing and specific dates of SST persistence, the reader is encouraged to visit www.remss.com/measurements/sea-surface-temperature/oisst-description.

2.2 Mapping the Polar Front

We build on the technique first presented by Moore et al. (1997) of using satellite SST gradient maxima to locate the PF. In general, our PF mapping technique is based on locating the southern bound at which the SST gradient exceeds 1.5°C over a 100 km distance, as in Dong et al. (2006b). At longitudes where this criterion cannot be satisfied or when large latitudinal distances exist between adjacent longitudes, steps are taken to satisfy spatial and/or thermal continuity, oftentimes as a relaxation of the above limit (see following subsections). Dong et al. (2006b) use 2σ and the temporal mean PF to identify such discontinuity. Here, we identify additional physical characteristics of the PF and use this information in a comprehensive mapping scheme. Our methodology does not require knowledge of a temporal mean PF; all information needed to map the PF is found locally. Our mapping scheme yields one continuous, unique PF realization for a given period of time. In regions where the PF is known to have multiple filaments (Sokolov and Rintoul, 2002), our algorithm typically selects the southernmost.

2.2.1 PF identification procedure

South of 40°S, we compute the absolute SST gradient (°C km^{-1}) at each grid point,

$$|\Delta T| = \sqrt{(\delta T/\delta x)^2 + (\delta T/\delta y)^2},$$

where δT is the temperature difference (°C) and δx and δy are the kilometer distances between any two longitude or latitude points, respectively. We do not perform initial, first-guess frontal identification (a) in regions where SST is warmer than 10°C, as these are waters characteristic of the SAF (Dong et al., 2006b), (b) within small patches of high SST gradients (closed contours less than 3 degrees of latitude and longitude), so as to reduce noise (as in Dong et al., 2006b), and (c) within 1 degree of latitude of the Antarctic continent or sea ice, in case of melt-influenced SSTs (Smith and Comiso, 2008).

2.2.2 Continuity tests

PF maps are checked for spatial and thermal continuity to determine whether an adjustment in the PF is necessary. Starting at the Greenwich Meridian and moving east, with the general flow of the ACC, we calculate the absolute differences (d) in latitude (l; °latitude), temperature (t; °C), and monthly climatological temperature (tc; °C) between the current position and the point to the west ($\leftarrow$) and east ($\rightarrow$), twice the standard deviation of these differences (normalized by N = 2), $2\sigma_l$ (°latitude) and $2\sigma_t$ and $2\sigma_{tc}$ (°C) respectively, and an additional difference (Δ) between 2σ and d (e.g., $\overleftarrow{\Delta_l}$ = | $\overleftarrow{d_l}$ - $2\sigma_l$ |). Invoking tc is necessary when injections of polar water from the south or subantarctic water from the north affect frontal identification.

An adjustment in the PF position is required if $2\sigma_l > 0.75$°latitude or ($2\sigma_l \leq 0.75$°latitude and ($\overleftarrow{\Delta_l} > 0.25$°latitude or $\overrightarrow{\Delta_l} > 0.25$°latitude)) and any of the following are satisfied:

$$\begin{cases} 2\sigma_l = \overleftarrow{d_l} \text{ and } (\overleftarrow{d_t} \geq 2\sigma_t \text{ or } \overleftarrow{d_{tc}} \geq 2\sigma_{tc}) & \\ \overleftarrow{d_l} < 2\sigma_l < \overrightarrow{d_l}, & \overrightarrow{\Delta_l} > 1 \\ 2\sigma_l < \overleftarrow{d_l} \text{ and } (2\sigma_t < \overleftarrow{d_t} \text{ or } 2\sigma_{tc} < \overleftarrow{d_{tc}}) & \\ 2\sigma_l < \overleftarrow{d_l} \text{ and } \overleftarrow{d_t} < 2\sigma_t < \overrightarrow{d_t}, & \overrightarrow{\Delta_t} > 1 \end{cases} \quad (1)$$

Figure 1 exemplifies spatial and thermal discontinuity according to (1) and shows the subsequent adjustment made in this particular case (adjustment procedure detailed in Section 2.2.3). Here, black plus signs indicate the first-guess PF position (i.e., the southern bound of the 1.5 temperature gradient criterion after removing noise/patches), where the current position being tested for continuity and its immediate neighbors to the west and east are indicated by black open circles. As spatial and thermal continuity is violated in this case (see difference and standard deviation information provided in text boxes), an adjustment in the PF position is made (white plus sign).

2.2.3 Adjustments

Following spatial and thermal continuity testing, we identify potential adjustment locations as those that satisfy $\overleftarrow{d_l} < 2\sigma_l$ and $\overrightarrow{\Delta_l} < 1$ (see Figure 1). Here, we locate the southernmost position of the 0.015°C km^{-1} absolute SST gradient. If a gradient of that magnitude is not found, we successively relax the gradient by 0.001°C km^{-1} to a lower limit of 0.011°C km^{-1} in order to find the front. In cases where gradients are relatively weak (i.e., $|\Delta T| < 0.011$°C km^{-1}), we use local gradient maxima (>0.008°C km^{-1}) to mark the position of the front.

In some cases, spatial or thermal discontinuity is justified. This generally occurs when two filaments are disconnected (Figure 2a; Sokolov and Rintoul, 2002), or when a branch of the front is predominantly situated north-south (Figure 2b).

2.2.4 Post-processing

In certain sectors of the Southern Ocean, the characteristics of the PF are such that mapping requires executing the above steps in the opposite direction, from east to west, in order to adequately capture the front's curled, folded, or multi-filament structure (Sokolov and Rintoul, 2002) or when it merges with or diverges from the SAF to the north (Read and Pollard, 1993;

Moore et al., 1997; Cunningham et al., 2003). The following areas of the Southern Ocean are often mapped as outlined in the previous subsections but from east to west: ∼20-32°E, ∼50-62°E near Crozet, ∼72-80°E near Kerguelen, ∼125-150°E along the Southeast Indian Ridge, ∼170-190°E in the New Zealand sector, ∼200-215°E along the Pacific-Antarctic Ridge, ∼240-300°E in the E. Pacific, and ∼352-360°E along the Mid-Atlantic Ridge.

3 Validating the PF position

In order to verify our methods, we compare realizations of PF location to those estimated from high-resolution XBT surface (<10 m) temperature data. XBT data are available from three Southern Ocean repeat lines: between Hobart, Australia and the Dumont d'Urville Station, Antarctica (line IX28; 64 transects; hereafter referred to as the Australian sector), across Drake Passage (line AX22; 73 transects), and another between Cape Town, South Africa and Sanae IV Station, Antarctica (line AX25; 25 transects; hereafter referred to as the African sector). We note that XBT sampling in the Australian and African sectors is biased to summer and spring seasons, whereas XBT data are collected year-round in the Drake Passage.

Along each transect, we interpolate the XBT SSTs to match the satellite grid resolution and compute meridional surface temperature gradients ($\delta T/\delta y$). We seek to find the in situ PF within one standard deviation of the weekly satellite PF location. In the African and Australian sectors, we identify the in situ PF as the southernmost latitude where $\delta T/\delta y \geq 0.015$°C km^{-1}. Given the strength of the SST gradient in Drake Passage, we adjust our definition to identify the southernmost latitude of the strongest $\delta T/\delta y$ exceeding 0.015°C km^{-1}.

We quantify the error associated with our PF mapping scheme in these three regions by calculating the root-mean-square error (RMSE), a measure of the average magnitude of the latitudinal differences between the PF inferred from XBT data (PF_X) and that from weekly microwave data (PF_M), as:

$$RMSE = \sqrt{\frac{\sum_{i=1}^{n}(PF_{X,i} - PF_{M,i})^2}{n}},$$

where n corresponds to the number of transects in a given sector. Table 1 lists RMSE and sample size by sector. Transects where a meridional temperature gradient satisfying our 0.015°C km^{-1} criterion could not be identified were excluded from these calculations (8 transects in total).

Differences between in situ and satellite PF locations are likely attributed to one or more of the following: (1) interpolating XBT SSTs on to the satellite grid, (2) differences in the representative temperature measured by the two sources ('bulk' versus 'subskin'; see Dong et al., 2006a), (3) errors in the original temperature data (e.g., manufacturer, accuracy, precision, etc.), (4) the regional complexity of the front (i.e., magnitude of mesoscale variability, typical number of branches, etc.), or (5) comparing a daily in situ PF with the corresponding weekly satellite PF.

The PF within the Australian and African sectors (RMSE 1.1640 and 0.7971° latitude, respectively; 2σ = 2.33 and 2.09° latitude, respectively), is known for its multi-filament structure (Belkin and Gordon, 1996; Moore et al., 1999; Sokolov and Rintoul, 2002, 2009b), making difficult the comparison between in situ and satellite-based definitions. For example, Figure 3a

shows more than one potential frontal location along a November 2003 transect south of Australia; the in situ PF is identified as the more northerly filament while our weekly PF realization marks the more southerly filament. Figure 3c shows a summertime African transect where the in situ PF is identified as a more southerly filament and our weekly realization represents the northern, more spatially continuous filament. In Drake Passage (RMSE = 0.5373° latitude; 2σ = 1.47° latitude), the PF is largely constrained by bathymetry (Moore et al., 1997) and characterized by an intense temperature gradient. Figure 3b shows a summertime Drake Passage transect where the in situ and satellite PF are identified one grid box apart (0.25° latitude). Such consistent identifications are reflected in the RMSE here, where on average, our mapping technique will provide PF positions within ∼0.5° latitude of an in situ position in a given week.

4 Results and discussion

We investigate the climatological position of the front by averaging weekly realizations over 2002-2014 (Figure 4, Figure 5). The climatological path of the PF is zonally asymmetric, traversing nearly 20° of latitude from its northernmost position in the southwest Indian Ocean (43.89°S) to its southernmost position in the southeast Pacific (64.08°S; Figure 4; Figure 5a). It follows that the climatological temperature along the path of the PF ranges from 0.6 to 6.9°C (Figure 4a; Figure 5b). The climatological intensity of the PF (defined as the absolute SST gradient at the front) averaged over all longitudes is 0.0173°C km^{-1}. Climatological intensity ranges from 0.0139 to 0.0225°C km^{-1} (Figure 4b; Figure 5c), possibly reflecting changes in ACC transport along the front (Dong et al., 2006b).

Figure 5 suggests that the mean position, temperature, and intensity of the PF are closely linked to the depth of the underlying topography (r = 0.43, r = 0.29, and r = 0.27, respectively), in agreement with previous PF studies (Gille, 1994; Moore et al., 1999; Sokolov and Rintoul, 2002; Dong et al., 2006b; Sallée et al., 2008). Indeed, the front tends to be southerly, cold, and weak over the deep ocean, and northerly, warm, and intense over shallow bathymetry. In the southwest Indian sector, the PF is in its northernmost position and characterized by warm SSTs (Figure 4; Figure 5a,b). Generally, the PF has a more southerly position in the deep, east Pacific sector, characterized by cooler SSTs and relatively weak SST gradients (Figure 4; Figure 5; Moore et al., 1999; Dong et al., 2006b). Figure 5c demonstrates that the PF intensifies at major topographic features, which are associated with strong, large-scale potential vorticity gradients that act to constrain the flow (Gordon et al., 1978; Sallée et al., 2008), including the Kerguelen Plateau (∼ 80°E), across the Southeast Indian Ridge (∼ 150°E), Drake Passage (∼ 60°W), and the Pacific-Antarctic Ridge (∼ 140°W).

We compare the climatological position of our PF with that estimated by the studies of Orsi et al. (1995), Belkin and Gordon (1996), Moore et al. (1999), and Dong et al. (2006b) in Figure 6, where the paths of the front are overlain on a map of bottom topography. The topographic influence on the position of the front is apparent: regions of strong topographic steering coincide with regions where all five climatological paths are in good agreement (e.g., along the Southeast Indian and Pacific-Antarctic Ridges in the New Zealand and Ross Sea sectors, through Drake Passage south of the Falkland Islands, and the eastern flank of Kerguelen Plateau) and these paths diverge from one another in deep ocean regions with weak to no topographic steering (e.g., the southeast Indian and Pacific basins).

Given the diversity in the methods and data used to identify the fronts shown in Figure 6, we do not expect the individual climatological paths to agree everywhere. For example, the Orsi et al. (1995) and Belkin and Gordon (1996) studies use hydrographic data to identify the front's subsurface expression, the northern extent of the 2°C isotherm at ∼200 m, while Moore et al. (1999) (Dong et al. (2006b)) identify the front as an SST gradient using infrared (microwave) satellite retrievals from 1987 to 1993 (2003 to 2005). Our climatological PF diverges most from that of Moore et al. (1999) in areas where persistent cloud cover contaminates the infrared SST retrieval (e.g., ∼50-70°E and ∼110-140°E). Since our study builds on the PF identification method presented in Dong et al. (2006b), it follows that the climatological position of our PF most closely matches that of Dong et al. (2006b).

Our climatological PF merges with the SAF north of the Crozet Archipelago (∼ 50°E), similar to (Dong et al., 2006b). It passes to the north of the Kerguelen Plateau (∼ 70°E), as in Orsi et al. (1995), Belkin and Gordon (1996), Dong et al. (2006b), and Sokolov and Rintoul (2009a). South of Crozet and Kerguelen, SST gradients are generally too weak to discern frontal filaments.

In the southeast Atlantic sector (330-350°E), our climatological PF extends further north than previous climatologies. This sector is characterized by many disconnected, smaller-scale frontal filaments south of the SAF. The continuity constraint in our method precludes identification of small-scale features as part of the PF, so here the PF follows the strongest and most coherent filament.

5 Conclusions

In summary, this study maps the Antarctic Polar Front from 2002 to 2014 at weekly resolution and provides the first temporally-varying PF data set derived from SST available to the scientific community. We outline a verified methodology to locate the PF throughout the Southern Ocean using the high-resolution, all-weather microwave SST data record. Further, we describe the climatological position, surface temperature, and intensity of the PF and compare our climatological PF to previous studies. As evidence for a variable and changing Southern Ocean grows (Gille, 2002; Böning et al., 2008; Cai et al., 2010; Munro et al., 2015b; Landschützer et al., 2015), determining the response of the PF to such changes is ever more crucial. For an investigation of intra-annual to interannual variability of the PF and associated drivers/mechanisms utilizing this high-resolution PF data set, the interested reader is encouraged to see our companion paper (Freeman and Lovenduski, in prep.).

6 PF data availability

Weekly PF locations can be found at http://doi.pangaea.de/10.1594/PANGAEA.855640 in netCDF (network Common Data Form) format and viewed as an animation.

Acknowledgements. Microwave OI SST data are produced by Remote Sensing Systems and sponsored by National Oceanographic Partnership Program (NOPP), the NASA Earth Science Physical Oceanography Program, and the NASA MEaSUREs DISCOVER Project. Drake

Passage and Australian sector XBT data were made available by the Scripps High Resolution XBT program (www-hrx.ucsd.edu). XBT data from the African sector were made available by the Atlantic Oceanographic and Meteorological Laboratory and are funded by the NOAA Office of Climate Observations. The Orsi et al. (1995) climatological PF position was obtained from the Australian Antarctic Data Center (Orsi and Harris, 2001). We thank S. Dong for providing her mean PF path. We are grateful for support from NSF (DGE-1144083; OCE-1155240; OCE-1258995) and NOAA (NA12OAR4310058).

References

Ansorge, I. J., Jackson, J. M., Reid, K., Durgadoo, J. V., Swart, S., and Eberenz, S.: Evidence of a southward eddy corridor in the south-west Indian ocean, Deep-Sea Res II, doi:10.1016/j.dsr2.2014.05.012, 2014.

Belkin, I. M. and Gordon, A. L.: Southern Ocean fronts from the Greenwich meridian to Tasmania, Journal of Geophysical Research, 101, 3675–3696, 1996.

Böning, C. W., Dispert, A., Visbeck, M., Rintoul, S. R., and Schwarzkopf, F. U.: The response of the Antarctic Circumpolar Current to recent climate change, Nature Geoscience, 1, 864–869, 2008.

Cai, W., Cowan, T., Godfrey, S., and Wijffels, S.: Simulations of Processes Associated with the Fast Warming Rate of the Southern Midlatitude Ocean, Journal of Climate, 23, 197–206, doi:10.1175/2009JCLI3081.1, 2010.

Cunningham, S. A., Alderson, S. G., and King, B. A.: Transport and variability of the Antarctic Circumpolar Current in Drake Passage, Journal of Geophysical Research, 108, 8084, 2003.

Deacon, G. E. R.: A general account of the hydrology of the South Atlantic Ocean, Discovery Rep., VII, 177–238, 1933.

Deacon, G. E. R.: The hydrology of the Southern Ocean, Discovery Rep., XV, 1–124, 1937.

Deacon, G. E. R.: Physical and biological zonation in the Southern Ocean, Deep-Sea Research, 29, 1–15, doi:10.1016/0198-0149(82)90058-9, 1982.

Dong, S., Gille, S. T., Sprintall, J., and Gentemann, C.: Validation of the Advanced Microwave Scanning Radiometer for the Earth Observing System (AMSR-E) sea surface temperature in the Southern Ocean, J. Geophys. Res., 111, doi:10.1029/2005JC002934, 2006a.

Dong, S., Sprintall, J., and Gille, S. T.: Location of the Antarctic Polar Front from AMSR-E Satellite Sea Surface Temperature Measurements, J. Phys. Oceanogr., 36, 2075–2089, 2006b.

Freeman, N. M. and Lovenduski, N. S.: Decreased calcification in the Southern Ocean over the satellite record, Geophysical Research Letters, doi:10.1002/2014GL062769, 2015.

Freeman, N. M. and Lovenduski, N. S.: Temporal variability in the Antarctic Polar Front (2002-2014), Journal of Geophysical Research: Oceans, in prep.

Gille, S. T.: Mean sea surface height of the Antarctic Circumpolar Current from Geosat data: Method and application, Journal of Geophysical Research, 99, 255–273, 1994.

Gille, S. T.: Warming of the Southern Ocean since the 1950s, Science, 295, 1275–1277, 2002.

Gordon, A. L., Molinelli, E., and Baker, T.: Large-Scale Relative Dynamic Topography of the Southern Ocean, Journal of Geophysical Research, 83, 1978.

Graham, R. M., de Boer, A. M., Heywood, K. J., Chapman, M. R., and Stevens, D. P.: Southern Ocean fronts: Controlled by wind or topography?, Journal of Geophysical Research: Oceans, 117, doi:10.1029/2012JC007887, 2012.

Hughes, C. W. and Ash, E. R.: Eddy forcing of the mean flow in the Southern Ocean, Journal of Geophysical Research: Oceans (1978–2012), 106, 2713–2722, doi:10.1029/2000JC900332, 2001.

Landschützer, P., Gruber, N., Haumann, F. A., Rodenbeck, C., Bakker, D. C. E., van Heuven, S., Hoppema, M., Metzl, N., Sweeny, C., Takahashi, T., Tilbrook, B., and Wanninkhof, R.: The reinvigoration of the Southern Ocean carbon sink, Science, 349, doi:10.1126/science.aab2620, 2015.

Legeckis, R.: Oceanic Polar Front in the Drake Passage - satellite observations during 1976, Deep-Sea Research, 24, 701–704, doi:10.1016/0146-6291(77)90510-0, 1977.

Mackintosh, N. A.: The Antarctic Convergence and the distribution of surface temperatures in Antarctic waters, Discovery Rep., XXIII, 177–212, 1946.

Moore, J. K., Abbott, M. R., and Richman, J. G.: Variability in the location of the Antarctic Polar Front (90^o-20^oW) from satellite sea surface temperature data, Journal of Geophysical Research, 102, 27,825–27,833, 1997.

Moore, J. K., Abbott, M. R., and Richman, J. G.: Location and dynamics of the Antarctic Polar Front from satellite sea surface temperature data, Journal of Geophysical Research: Oceans, 104, 3059–3073, doi:10.1029/1998JC900032, 1999.

Munro, D. R., Lovenduski, N. S., Stephens, B. B., Newberger, T., Arrigo, K. R., Takahashi, T., Quay, P. D., Sprintall, J., Freeman, N. M., and Sweeney, C.: Estimates of net community production in the Southern Ocean determined from time series observations (2002-2011) of nutrients, dissolved inorganic carbon, and surface ocean pCO_2 in Drake Passage, Deep-Sea Res II, 114, 49–63, doi:10.1016/j.dsr2.2014.12.014, 2015a.

Munro, D. R., Lovenduski, N. S., Takahashi, T., Stephens, B. B., Newberger, T., and Sweeney, C.: Recent evidence for a strengthening CO_2 sink in the Southern Ocean from carbonate system measurements in the Drake Passage (2002-2015), Geophysical Research Letters, 42, doi:10.1002/2015GL065194, 2015b.

Orsi, A. H. and Harris, U.: Locations of the various fronts in the Southern Ocean, Australian Antarctic Data Centre - CAASM Metadata, https://data.aad.gov.au/aadc/metadata/metadata_redirect.cfm?md=/AMD/AU/southern_ocean_fronts, 2001.

Orsi, A. H., III, T. W., and Jr., W. D. N.: On the meridional extent and fronts of the Antarctic Circumpolar Current, Deep Sea Research Part I: Oceanographic Research Papers, 42, 641–673, doi:10.1016/0967-0637(95)00021-W, 1995.

Pollard, R. T., Lucas, M. I., and Read, J. F.: Physical controls on biogeochemical zonation in the Southern Ocean, Deep Sea Research Part II, 49, 3289–3305, 2002.

Read, J. F. and Pollard, R. T.: Structure and Transport of the Antarctic Circumpolar Current and Agulhas Return Current at 40^oE, Journal of Geophysical Research: Oceans (1978–2012), 98, 12,281–12,295, 1993.

Reynolds, R. W. and Smith, T. M.: Improved Global Sea Surface Temperature Analyses Using Optimum Interpolation, Journal of Climate, 7, 929–948, 1994.

Rintoul, S. R., Hughes, C., and Olbers, D.: The Antarctic Circumpolar Current System, in: Ocean Circulation and Climate, edited by Siedler, G., Church, J., and Gould, J., pp. 271–302, Academic Press, 2001.

Sallée, J. B., Speer, K., and Morrow, R.: Response of the Antarctic Circumpolar Current to Atmospheric Variability, Journal of Climate, 21, 3020–3039, 2008.

Sarmiento, J. L., Gruber, N., Brzezinski, M. A., and Dunne, J. P.: High-latitude controls of thermocline nutrients and low latitude biological productivity, Nature, 427, 56–60, 2004.

Smith, W. O. and Comiso, J. C.: Influence of sea ice on primary production in the Southern Ocean: A satellite perspective, Journal of Geophysical Research: Oceans (1978–2012), 113, 2008.

Sokolov, S. and Rintoul, S. R.: Structure of Southern Ocean fronts at 140^oE, Journal of Marine Systems, 37, 151–184, 2002.

Sokolov, S. and Rintoul, S. R.: Multiple Jets of the Antarctic Circumpolar Current South of Australia, Journal of Physical Oceanography, 37, 1394–1412, doi:10.1175/JPO3111.1, 2007.

Sokolov, S. and Rintoul, S. R.: Circumpolar structure and distribution of the Antarctic Circumpolar Current fronts: 2. Variability and relationship to sea surface height, J. Geophys. Res., 14, 2009a.

Sokolov, S. and Rintoul, S. R.: Circumpolar structure and distribution of the Antarctic Circumpolar Current fronts: 1. Mean circumpolar paths, Journal of Geophysical Research, 114, doi:10.1029/2008JC005108, 2009b.

Trull, T. W., Rintoul, S. R., Hadfield, M., and Abraham, E. R.: Circulation and seasonal evolution of polar waters south of Australia: implications for iron fertilization of the Southern Ocean., Deep-Sea Res., Part II, 48, 2439–2466, 2001.

Table 1. Estimated PF location RMS error (degrees of latitude) and sample size (n), by sector.

	RMSE	n
Australian sector	1.1640	59
Drake Passage	0.5373	71
African sector	0.7971	24

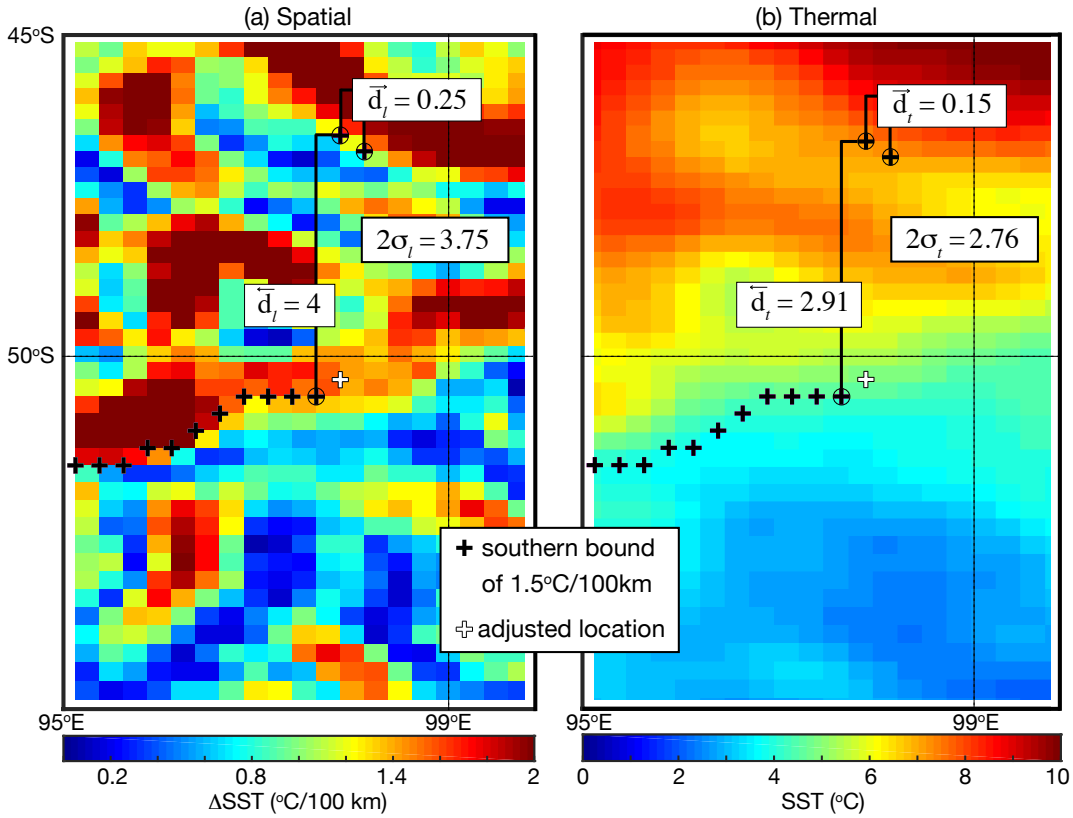

Figure 1. Example of (a) spatial and (b) thermal discontinuity resulting in an adjustment in the PF location according to (1) as outlined in Section 2.2.2. d_l, $2\sigma_l$ in units of °latitude and d_t, $2\sigma_t$ in units of °C.

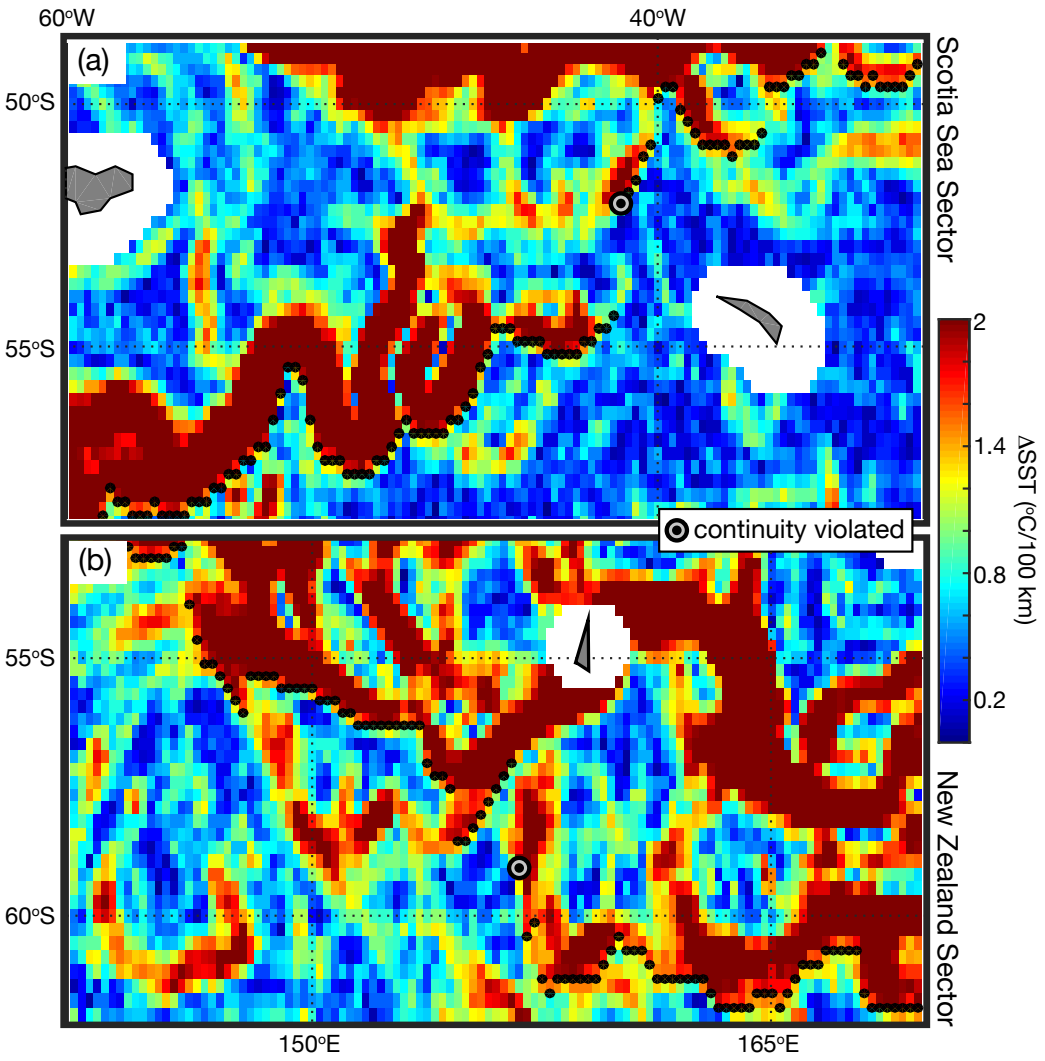

Figure 2. Example cases when spatial and thermal discontinuity is justified: frontal filaments (a) disconnected or (b) situated north-south.

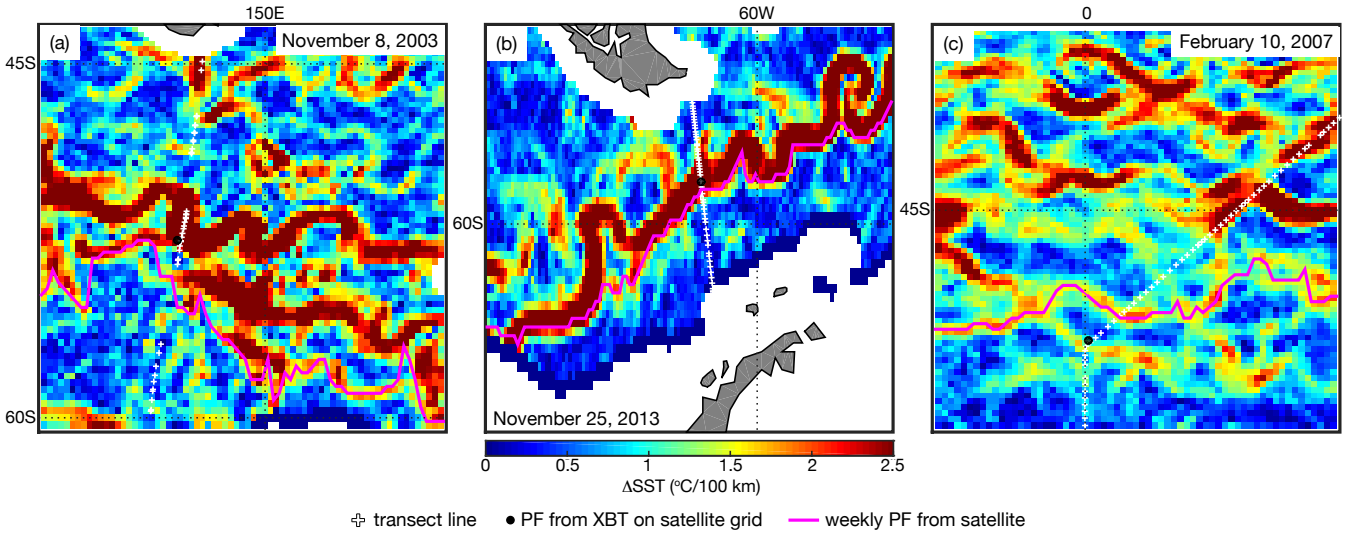

Figure 3. PF location identified from surface XBT data (timestamp indicated) overlain on the corresponding weekly satellite-estimated ΔSST and PF realization in the (a) Australian, (b) Drake Passage, and (c) African sectors.

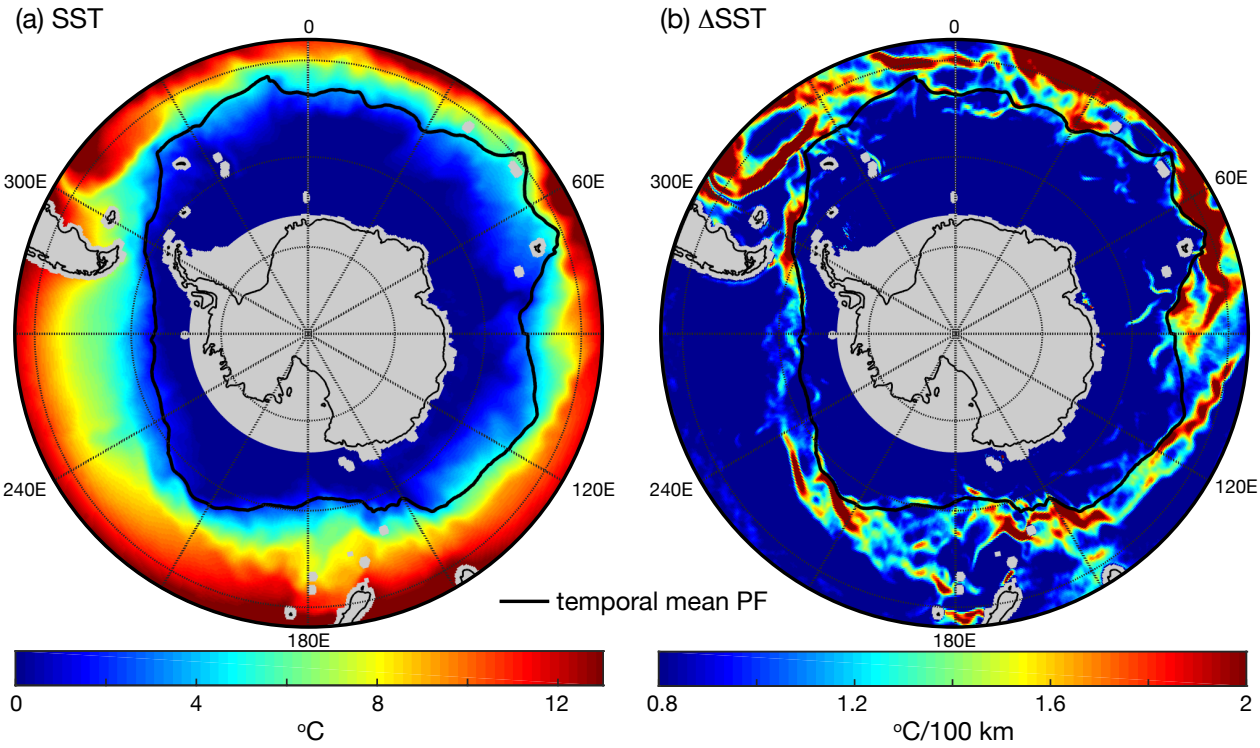

Figure 4. Southern Ocean (a) mean SST and (b) absolute SST gradient with climatological PF overlain (June 2002-February 2014).

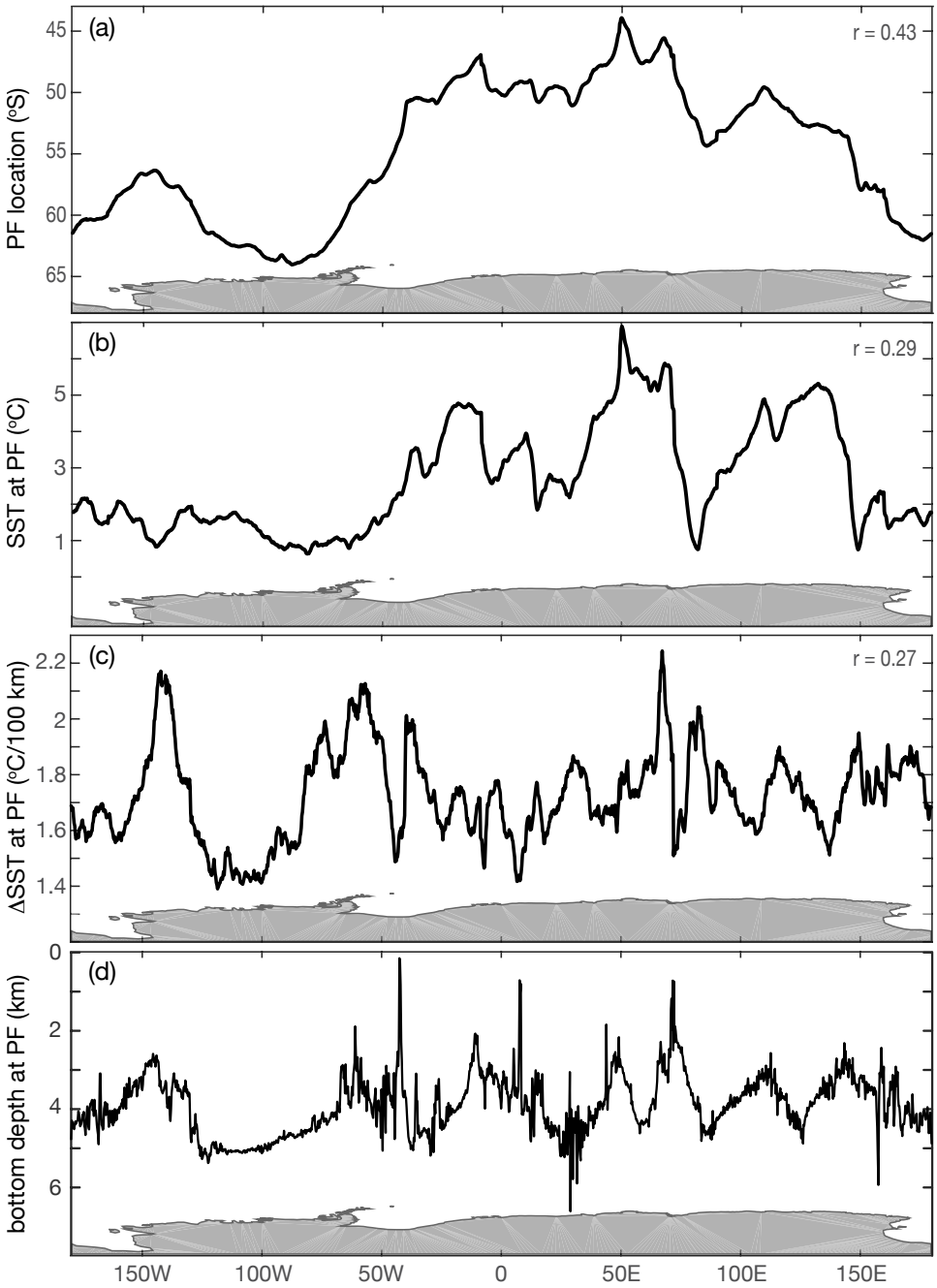

Figure 5. Climatological (a) PF location and (b) SST, (c) absolute SST gradient, and (d) bottom depth at the PF (June 2002-February 2014). Statistically significant (>95%) correlation coefficients with bottom depth are indicated in the top right corner of (a-c).

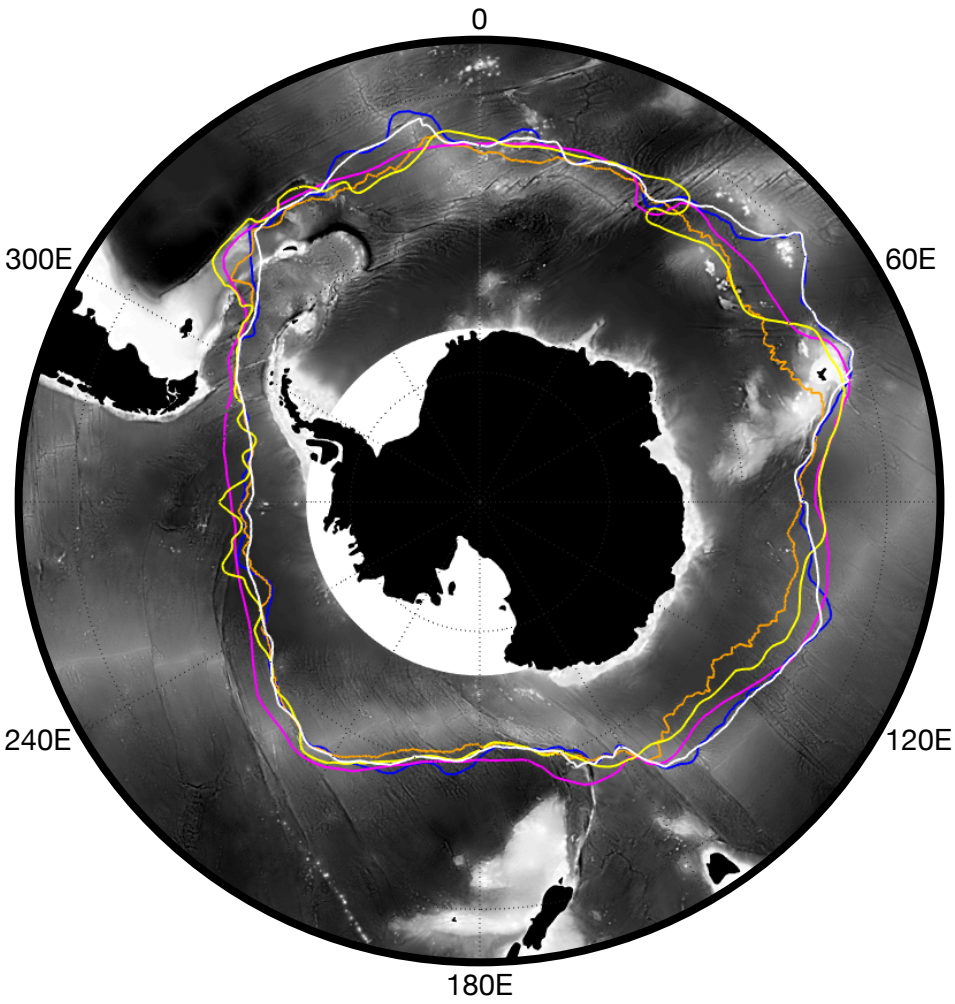

Figure 6. The climatological position of the PF in this and previous studies overlain on bottom topography, where light (dark) shading indicates shallow (deep) bathymetry.